A Hybrid Method for Source Direction Finding with Radio Frequency Interference and Gaussian White Noise

Yanming Zhang, *Member, IEEE*, Wenchao Xu, *Senior Member, IEEE*, Antonios Argyriou, *Senior Member, IEEE*, A-Long Jin, *Member, IEEE*, Tianquan Tang, Peifeng Ma, *Senior Member, IEEE*, Lijun Jiang, *Fellow, IEEE*, and Steven Gao, *Fellow, IEEE*

***Abstract*—This paper presents a hybrid data-driven method, termed moving average-Hankel-dynamic mode decomposition (MAHankDMD), for joint direction of arrival (DOA) and frequency estimation in environments affected by both radio frequency interference (RFI) and Gaussian white noise. The proposed approach integrates two key components: (1) a moving average-DMD filter that effectively mitigates Gaussian white noise and separates RFI from the source signal, and (2) a Hankel-DMD method that accurately estimates the DOA of the filtered signal and associates it with the corresponding frequency. The moving average-DMD stage first enhances the signal-to-noise ratio and improves the robustness of the estimation process through noise and inference mitigation, while the subsequent Hankel-DMD stage enables reliable parameter extraction even for overlapping sginals or strong interference conditions. Numerical simulations demonstrate the robustness of MAHankDMD, showing its ability to precisely estimate both DOA and frequency under challenging conditions involving RFI and Gaussian white noise interference. The proposed algorithm thus provides an effective solution for channel parameter estimation in complex noisy environments.**

***Index Terms*—Radio frequency interference, Gaussian white noise, direction of arrival, joint estimation, moving average filter, dynamic mode decomposition.**

This work is supported in part by Chinese University of Hong Kong Startup Fund under Grant 4937123, Grant 4937124, Grant 14223422, Grant 14201923, Grant 4937125, Grant 4937126, Grant 8601743, and Grant 4055185, in part by the Research Grants Council of the Hong Kong Special Administrative Region under Project No. PolyU15225023, in part by the XJTLU Research Development Fund under Project No. RDF-23-02-064, in part by the Research Grants Council of Hong Kong under Grant GRF 14210623, in part by ITF Grant ITP/007/23LP, and in part by RGC Grant AoE/E-101/23-N and AoE/E-603/18.*(Corresponding author: A-Long Jin)*

Yanming Zhang and Steven Gao are with the Department of Electronic Engineering, The Chinese University of Hong Kong, Hong Kong, China (e-mail: ymzhang@eee.hku.hk; scgao@ee.cuhk.edu.hk).

Wenchao Xu is with the Division of Integrative Systems and Design, Hong Kong University of Science and Technology, Hong Kong, China (e-mail: wenchaoxu@ust.hk).

Antonios Argyriou is with the Department of Electrical and Computer Engineering, University of Thessaly, 38221, Volos, Greece (e-mail: anargyr@uth.gr)

A-Long Jin is with the Department of Communications and Networking, Xi'an Jiaotong-Liverpool University, Suzhou 215123, China (e-mail: along.jin@xjtlu.edu.cn).

Tianquan Tang is with the Lab for Aerodynamics and Acoustics, HKU Zhejiang Institute of Research and Innovation, Hangzhou, China (e-mail: tianquan@connect.hku.hk).

Peifeng Ma is with Department of Geography and Resource Management, Institute of Space and Earth Information Science, The Chinese University of Hong Kong, Shatin, NT, Hong Kong (e-mail: mapeifeng@cuhk.edu.hk).

Lijun Jiang is with the Department of Electrical and Computer Engineering, Missouri University of Science and Technology, Rolla, MO, USA (e-mail: ljf82@mst.edu).

I. Introduction

Within cognitive radio technology, the simultaneous estimation of direction of arrival (DOA) and frequency plays a critical role in enhancing spectral utilization efficiency [1], [2] and improving localization accuracy [3], [4], [5], [6]. This joint estimation process has attracted increasing attention due to its capacity to improve both spatial and temporal sensing of the communication environment, thereby strengthening link quality [7], [8], [9]. To address the joint DOA and frequency estimation problem, numerous methods have been developed, including Jacobi rotation [10], general single-pole autoregressive moving-average model [11], estimation of signal parameters via rotational invariant techniques (ESPRIT) with sub-Nyquist sampling [5], [12], 2D multiple signal classification (MUSIC) [13], convolutional neural network (CNN)-based methods [14], [15]. These methods have achieved notable success in extracting signal parameters under various conditions. However, some challenges remain, such as the need for parameter matching after estimation [16], the assumption of a known number of sources [17], or sensitivity to interference and noise [18]. These open problems suggest that there is still a need for the development of more flexible and robust techniques that can perform reliably across a wider range of practical scenarios.

Another major challenge arises from the pervasive presence of noise and interference in practical signal environments. Existing methods such as spatial smoothing [19], Kalman filtering [20], and time-frequency analysis [21] are effective for mitigating Gaussian noise, but often struggle with structured interference like radio frequency interference (RFI). RFI, which may stem from hardware imperfections or intentional jamming [22], [23], can significantly degrade estimation performance by contaminating the spectral environment. This leads to increased uncertainty and reduced communication reliability [24], [25]. The problem is especially critical in cognitive radio systems, where accurate spectrum sensing is essential for enabling dynamic access and avoiding interference [26]. Fig. 1 illustrates the conceptual challenge of joint DOA and frequency estimation in the presence of both sources and RFI. In this scenario, signals are transmitted simultaneously toward a uniform linear array (ULA) from multiple directions, with terrestrial base stations representing the sources of interest (SOIs) and low-altitude UAVs representing

RFI. While the goal is to localize and track the SOIs, the presence of RFI complicates this process, as interfering signals obscure the spectral and spatial features of the SOIs. In addition to structured signals such as RFI, Gaussian white noise represents another significant factor that impairs estimation performance [27], [28]. In high-noise environments, Gaussian white noise can overwhelm the true SOIs' signal components, further compromising the accuracy of DOA and frequency estimation. When the noise power is sufficiently high, it becomes increasingly difficult to resolve weak signal features, thereby necessitating noise-resilient estimation strategies [29]. While existing dynamic mode decomposition (DMD)-based methods offer powerful modal analysis tools, they suffer from sensitivity to Gaussian noise and structured interference [30], [31]. These challenges highlight the need for the development of more robust and adaptive joint estimation methods that can effectively operate under complex interference and noise conditions.

In this paper, we propose a moving average-Hankel-dynamic mode decomposition (MAHankDMD) approach to jointly estimate the DOA and frequency of multiple narrowband sources in environments contaminated by both RFI and Gaussian white noise. The proposed framework performs simultaneous DOA and frequency estimation from the space-time signals received by a ULA. It enables the identification of both SOIs and RFI, provided that their frequency differences are known in advance. The proposed method accurately pairs each frequency component with its corresponding spatial angle, enabling the separation of useful signals from interference. The main contributions are highlighted as follows:

1) We introduce the hybrid framework, MAHankDMD, for joint DOA and frequency estimation in the presence of RFI and Gaussian white noise. With this approach, frequencies and DOA are extracted directly from the eigenvalues and eigenvectors, respectively. As each eigenvalue-eigenvector pair corresponds to a distinct signal component, the method inherently achieves pairing-free estimation, eliminating the need for additional parameter matching procedures.
2) The moving average filter is incorporated into our proposed MAHankDMD framework to preprocess the spatial-temporal signal prior to decomposition. This filtering step reduces the impact of Gaussian white noise and stabilizes the input data. By enhancing the signal-to-noise (SNR) ratio before dynamic mode extraction, the moving average filter substantially improves the robustness of the estimation process. Comparative experiments show that, particularly under low SNR conditions, the MAHankDMD method with moving average filtering achieves significantly better performance than standard DMD in terms of both stability and estimation accuracy.
3) The proposed framework allows for the precise retrieval of one-dimensional spatial distributions for both SOI and RFI. By adopting an augmented Hankel structure, our method facilitates the accurate extraction of multiple signal directions from the one-dimensional spatial profiles. Also, as the number of antennas increases, the spatial resolution improves, leading to enhanced DOA estimation accuracy. This approach could prove particularly effective in scenarios involving overlapping signals or strong interference.

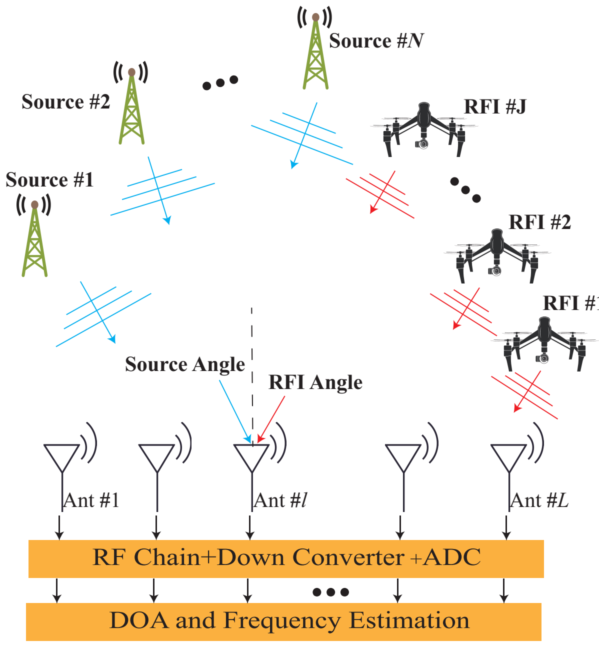

Fig. 1. Illustration of simultaneous frequency and DOA estimation with interference from low-altitude UAVs and signal sources from base stations.

The remainder of this article is organized as follows. Section II provides a detailed formulation of the problem. Section III introduces the proposed MAHankDMD method and elaborates on its implementation. Section IV presents several benchmark examples to validate the effectiveness of the proposed approach. Finally, Section V concludes this work.

II. Problem Formulation

We consider a uniform linear array (ULA) consisting of L omnidirectional sensors receiving I narrowband signals $s_i(t)$, where $i = 1, 2, \ldots, I$, and t denotes the time variable. The sources are assumed to be in the far field with unknown directions of arrival $\theta_i, i = 1, 2, \ldots, I$. Assuming identical sensors and no location uncertainties, the ideal steering vector for a direction θ is given by:

$$\mathbf{a}(\theta) = \left[1, \alpha(\theta), \ldots, \alpha(\theta)^{L-1}\right]^{\mathrm{T}}, \tag{1}$$

where $\alpha(\theta) = \exp\left(-j_0 2\pi \lambda_s^{-1} d \sin\theta\right)$, with d being the inter-sensor spacing, λ_s the source signal wavelength, $j_0 = \sqrt{-1}$ and $(\cdot)^{\mathrm{T}}$ indicating the transpose. The observed array output vector $\mathbf{x}(t)$ can be expressed as follows:

$$\mathbf{x}(t) = \mathbf{A}\mathbf{s}(t), \tag{2}$$

where $\mathbf{A} = [\mathbf{a}(\theta_1), \mathbf{a}(\theta_2), \ldots, \mathbf{a}(\theta_I)]$ and $\mathbf{s}(t) = [s_1(t), s_2(t), \ldots, s_I(t)]^{\mathrm{T}}$. $\mathbf{A}$ means the ideal steering matrix and $\mathbf{s}(t)$ is the vector of signal waveforms. Herein, $s_i(t)$ includes also the channel fading coefficient $u_i(t)$, namely

$s_i(t) = u_i(t)e^{j_0(\omega_i t+\varphi_i)}$. Then, the received signal model at the l-th antenna is given by

$$x_l(t) = \sum_{i}^{I} a_l(\theta_i)s_i(t) = \sum_{i}^{I} a_l(\theta_i)u_i(t)e^{j_0(\omega_i t+\phi(t))}. \quad (3)$$

With the presence of RFI sources in the channel, the signals received by the ULA not only contain the desired signals but also include RFI components. To extend the model by incorporating RFI, we consider the presence of J narrowband interferers $r_j(t)$, where $j = 1, 2, \cdots, J$. These interference signals $r_j(t)$ originate from independent sources, each with an unknown DOA ϕ_j, assumed to be distinct from the source signal directions θ_i, as shown in Fig. 1. The steering vector for a direction ϕ_j corresponding to the j-th interferer can be expressed as:

$$\mathbf{b}(\phi) = \left[1, \beta(\phi), \ldots, \beta(\phi)^{L-1}\right]^{\mathrm{T}}, \quad (4)$$

where $\beta(\phi) = \exp\left(-j_0 2\pi\lambda_r^{-1} d \sin\phi\right)$ is similar to the signal steering vector, but defined for the interferer directions. The interference signals $r_j(t)$ are modeled as generic narrowband sinusoidal tones with random amplitude fading and phases: $r_j(t) = v_j(t)e^{j_0(\vartheta_j t+\varphi_j)}$, so that we can capture any type of RFI. Herein, v_j, ϑ_j, and φ_j denote the narrowband fading channel coefficient, frequency, and phase for the j-th interferer. The array output vector $\mathbf{x}(t)$ is thus augmented to include both the desired signals and interference signals as follows:

$$\mathbf{y}(t) = \mathbf{A}\mathbf{s}(t) + \mathbf{B}\mathbf{r}(t), \quad (5)$$

where $\mathbf{B} = [\mathbf{b}(\phi_1), \mathbf{b}(\phi_2), \ldots, \mathbf{b}(\phi_J)]$ is the steering matrix for the interferers, $\mathbf{r}(t) = [r_1(t), r_2(t), \ldots, r_J(t)]^{\mathrm{T}}$ is the vector of interference signals.

Additionally, additive white Gaussian noise (AWGN) is one of the most common types of impairments in wireless communication systems. It could originate from thermal noise in electronic components, environmental electromagnetic e-missions, and other random fluctuations. Generally, Gaussian white noise is characterized by random fluctuations with a flat spectral density and zero-mean Gaussian distribution [5], [6], which degrades the signal-to-noise ratio (SNR) and thereby worsens the accuracy of angle estimation. Mathematically, it can be described as:

$$\mathbf{n}(t) = [n_1(t), n_2(t), \ldots, n_L(t)]^{\mathrm{T}}, \quad (6)$$

where $n_l(t)$ is the noise observed at the l-th sensor. Each $n_l(t)$ is modeled as a zero-mean complex Gaussian random process, namely $n_l(t) \sim \mathcal{CN}\left(0, \sigma^2\right)$. $\mathcal{CN}\left(0, \sigma^2\right)$ denotes a circularly symmetric complex Gaussian distribution. And σ^2 means the noise power, which is typically assumed identical across all array elements for simplicity. Then, the complete received signal model can be obtained as

$$\mathbf{z}(t) = \mathbf{A}\mathbf{s}(t) + \mathbf{B}\mathbf{r}(t) + \mathbf{n}(t). \quad (7)$$

That is to say, incorporating the desired signals, narrowband RFI components, and additive noise, the received signal at the l-th antenna is:

$$z_l(t) = \sum_{i=1}^{I} a_l(\theta_i) s_i(t) + \sum_{j=1}^{J} b_l(\phi_j) r_j(t) + n_l(t). \quad (8)$$

The primary objective of this study is to estimate the DOA, denoted by θ_i, and the corresponding source frequencies in the presence of RFI and Gaussian white noise. This estimation is critical for robust signal processing and reliable performance in practical communication systems affected by complex interference environments.

III. Methodology

The proposed methodology integrates a moving average filter for Gaussian with noise suppression and a Hankel-DMD for robust DOA estimation. This section first introduces the traditional DMD and then the moving average-DMD, followed by the proposed MAHankDMD approach for the DOA and frequency estimation in the presence of RFI and Gaussian white noise.

A. Dynamic Mode Decomposition

According to (7), the received spatial-temporal signal of the ULA with a $T+1$ time period can be obtained as

$$\mathbf{Z} = \left[\begin{array}{ccccc} \mathbf{z}_0 & \cdots & \mathbf{z}_t & \cdots & \mathbf{z}_T \end{array}\right] \in \mathbb{C}^{L\times(T+1)}, \quad (9)$$

where $\mathbf{z}_t = [z_1(t), \cdots, z_l(t), \cdots, z_L(t)]^T \in \mathbb{C}^{L\times 1}$. The traditional DMD is a purely data-driven method designed to build the governing equation based on the received data. In particular, the received spatial-temporal signal, $\mathbf{Z}$, is initially reshaped into two adjacent matrices:

$$\mathbf{Z}_1 = \left[\begin{array}{ccccc} \mathbf{z}_0 & \cdots & \mathbf{z}_t & \cdots & \mathbf{z}_{T-1} \end{array}\right] \in \mathbb{C}^{M\times T}, \quad (10)$$

$$\mathbf{Z}_2 = \left[\begin{array}{ccccc} \mathbf{z}_1 & \cdots & \mathbf{z}_t & \cdots & \mathbf{z}_T \end{array}\right] \in \mathbb{C}^{M\times T}. \quad (11)$$

Based on the linear assumption between two adjacent states, i.e., $\mathbf{z}_{t+1} = \mathbf{F}\mathbf{z}_t$, the relationship between (10) and (11) can be expressed as $\mathbf{Z}_2 = \mathbf{F}\mathbf{Z}_1$. Herein, $\mathbf{F}$ refers to the mapping matrix, and the purpose of DMD is to calculate the leading eigenvalues and eigenvectors of $\mathbf{F}$. Singular value decomposition (SVD) is used to implement the DMD steps [32]. Initially, we apply the SVD to the first matrix $\mathbf{Z}_1$, which is expressed as

$$\mathbf{Z}_1 = \mathbf{U}\boldsymbol{\Sigma}\mathbf{V}^*, \quad (12)$$

where $*$ denotes the conjugate transpose. By substituting (12) into $\mathbf{Z}_2 = \mathbf{F}\mathbf{Z}_1$, we can derive the mapping matrix $\mathbf{F}$ as

$$\mathbf{F} = \mathbf{Z}_2\mathbf{V}\boldsymbol{\Sigma}^{-1}\mathbf{U}^*. \quad (13)$$

Then, $\mathbf{U}$ is employed to project the original system into a corresponding reduced-dimensional system. Specifically, the original snapshots are transformed using the proper orthog-onal decomposition (POD) basis. It can be represented as $\hat{\mathbf{Z}}_1 = \mathbf{U}^*\mathbf{Z}_1$ and $\hat{\mathbf{Z}}_2 = \mathbf{U}^*\mathbf{Z}_2$. In this reduced-dimensional system, indicated by the notation $(\hat{\cdot})$, we define the transfor-mation matrix $\hat{\mathbf{F}} = \mathbf{U}^*\mathbf{F}\mathbf{U}$. Consequently, we can express the mapping relationship in the reduced-dimensional system by:

$$\hat{\mathbf{Z}}_2 = \hat{\mathbf{F}}\hat{\mathbf{Z}}_1. \quad (14)$$

Importantly, the mapping matrix $\hat{\mathbf{F}}$ in the reduced-dimensional system effectively captures dynamic characteristics. We then

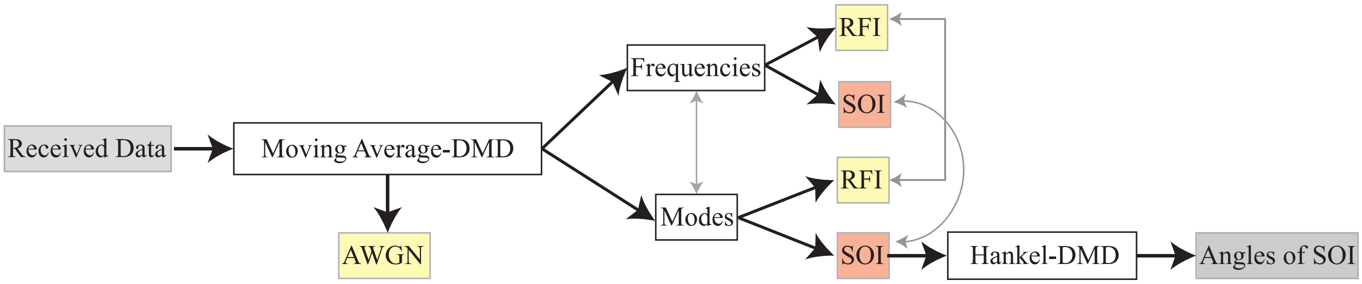

Fig. 2. Flowchart of the proposed MAHankDMD method.

address the eigenvalue problem in this compressed framework by performing an eigendecomposition of $\hat{\mathbf{F}}$:

$$\hat{\mathbf{F}}\mathbf{D} = \mathbf{D}\mathbf{\Lambda}, \tag{15}$$

where $\mathbf{D}$ consists of the eigenvectors of $\hat{\mathbf{F}}$, and $\mathbf{\Lambda}$, a diagonal matrix, contains the eigenvalues, denoted as λ_k for $k = 1, 2, ..., K$. Leveraging these results, we define the DMD eigenvectors in the original system as follows:

$$\mathbf{G} = \mathbf{Z}_2\mathbf{V}\mathbf{\Sigma}^{-1}\mathbf{D}. \tag{16}$$

The data at a given time can be represented as:

$$\mathbf{z}_t = \sum_{k=1}^{K} \mathbf{g}_k b_k e^{\omega_k t}. \tag{17}$$

Here, $\mathbf{g}_k$ is the k-th column of the matrix $\mathbf{G}$, and $\omega_k = \text{real}(\omega_k) + j_0\text{imag}(\omega_k) = \ln(\lambda_k)/\Delta t$.

By comparing the DMD expression of the data, namely (17), to a standard signal model, namely (7), we can deduce the frequencies of both source signals (ω_i) and interference signals (ϑ_j) from the distribution of ω_k. Assuming prior partial knowledge of the frequencies or the identities of SOI and RFI, we can categorize the SOI and RFI based on the calculated values of ω_k. That is to say, we have determined the frequency distribution, but we have not yet estimated the angles. Additionally, due to the interference from RFI and Gaussian noise, accurately estimating these frequencies presents a challenge. Therefore, in the next subsections, we will use the moving averaging technique to eliminate the interference from Gaussian white noise and the Hankel DMD for the angle estimation.

B. Moving Average-Dynamic Mode Decomposition

The moving average technique is a well-established method for mitigating the impact of Gaussian white noise in signal processing [19], [33]. Herein, by averaging adjacent columns of the data matrix, the random fluctuations caused by noise are smoothed out, while the underlying signal structure is preserved. This could be particularly useful in the context of the DMD method, a purely data-driven method, where the accuracy of computed eigenvalues and eigenvectors depends on the quality of the input data. Herein, we refer to this hybrid approach as moving average-DMD.

Specifically, given the received data matrix $\mathbf{Z}$, the moving average is applied by summing and averaging ζ consecutive columns. Mathematically, ζ refers to the window size of the moving average filter. For a temporal signal at times t_q, $t_q + \Delta t, \cdots, t_q + (\zeta - 1)\Delta t$, the moving average process can be defined as:

$$\overline{\overline{\mathbf{z}}}_q = \frac{1}{\zeta}\sum_{i=0}^{\zeta-1} \mathbf{z}\left(t_q + i\Delta t\right), \tag{18}$$

where $\overline{\overline{\mathbf{z}}}_q$ represents the smoothed signal at time t_q. Substituting (8) into (18), one can obtain:

$$\begin{aligned}\overline{\overline{\mathbf{z}}}_q =& \frac{1}{\zeta}\sum_{i=0}^{\zeta-1} \mathbf{x}\left(t_q + i\Delta t\right) + \frac{1}{\zeta}\sum_{i=0}^{\zeta-1} \mathbf{y}\left(t_q + i\Delta t\right) \\ &+ \frac{1}{\zeta}\sum_{i=0}^{\zeta-1} \mathbf{n}\left(t_q + i\Delta t\right) \\ =& \overline{\overline{\mathbf{x}}}_q + \overline{\overline{\mathbf{y}}}_q + \overline{\overline{\mathbf{n}}}_q.\end{aligned} \tag{19}$$

Herein, $\frac{1}{\zeta}\sum_{i=0}^{\zeta-1} \mathbf{x}\left(t_q + i\Delta t\right) = \overline{\overline{\mathbf{x}}}_q$, $\frac{1}{\zeta}\sum_{i=0}^{\zeta-1} \mathbf{y}\left(t_q + i\Delta t\right) = \overline{\overline{\mathbf{y}}}_q$, and $\frac{1}{\zeta}\sum_{i=0}^{\zeta-1} \mathbf{n}\left(t_q + i\Delta t\right) = \overline{\overline{\mathbf{n}}}_q$. $\overline{\overline{\mathbf{x}}}_q$, $\overline{\overline{\mathbf{y}}}_q$, and $\overline{\overline{\mathbf{n}}}_q$ refer to the smoothed true signal component, smoothed RFI component, and smoothed noise, respectively. Due to the zero-mean property of Gaussian noise, the moving average reduces the noise variance by a factor of ζ, effectively attenuating its impact:

$$\text{Variance of } \overline{\overline{\mathbf{n}}}_q = \frac{\sigma^2}{\zeta}. \tag{20}$$

Clearly, the variance of the original noise σ^2 is reduced to $\frac{\sigma^2}{\zeta}$. By choosing an appropriate window size ζ, we ensure sufficient noise suppression without distorting the temporal resolution of the signal. Notably, the selection of the window size ζ is critical. It should be sufficiently large to achieve noise suppression, but not so large that it distorts the underlying signal dynamics. A general guideline is to ensure ζ is smaller than one-quarter of the shortest signal period:

$$\zeta < \frac{T_{min}}{4\Delta t}, \tag{21}$$

where T_{min} is the minimum signal period of interest, and Δt is the sampling interval. This ensures the moving average primarily reduces noise while preserving the temporal resolution of the signal.

Next, the moving average is integrated to the DMD framework as a preprocessing step to refine the data matrices $\mathbf{Z}_1$ and $\mathbf{Z}_2$. For a received signal $\mathbf{Z}$, the smoothed data matrices $\overline{\overline{\mathbf{Z}}}_1$ and $\overline{\overline{\mathbf{Z}}}_2$ are constructed by replacing each column with the averaged values over the window size ζ as:

$$\overline{\overline{\mathbf{Z}}}_1 = \left[\overline{\overline{\mathbf{z}}}_0, \overline{\overline{\mathbf{z}}}_1, \ldots, \overline{\overline{\mathbf{z}}}_{T-\zeta-1}\right], \tag{22}$$

$$\overline{\overline{\mathbf{Z}}}_2 = \left[\overline{\overline{\mathbf{z}}}_1, \overline{\overline{\mathbf{z}}}_2, \ldots, \overline{\overline{\mathbf{z}}}_{T-\zeta}\right]. \tag{23}$$

After applying the moving average, the smoothed data matrices $\overline{\overline{\mathbf{Z}}}_1$ and $\overline{\overline{\mathbf{Z}}}_2$ are used in place of the original matrices, i.e., (10) and (11) in the DMD process. To be specific, we first perform SVD on $\overline{\overline{\mathbf{Z}}}_1$:

$$\overline{\overline{\mathbf{Z}}}_1 = \overline{\overline{\mathbf{U}}}\,\overline{\overline{\mathbf{\Sigma}}}\,\overline{\overline{\mathbf{V}}}^*. \tag{24}$$

Then, the mapping matrix $\overline{\overline{\mathbf{F}}}$ can be computed as follows:

$$\overline{\overline{\mathbf{F}}} = \overline{\overline{\mathbf{Z}}}_2\overline{\overline{\mathbf{V}}}\,\overline{\overline{\mathbf{\Sigma}}}^{-1}\overline{\overline{\mathbf{U}}}^*. \tag{25}$$

Next, $\overline{\overline{\mathbf{U}}}$ is used to project the original system into its corresponding low-rank one. After that, we adopt the eigendecomposition of $\overline{\overline{\mathbf{F}}}$ in the low-rank system to extract the system's dynamic modes and frequencies. Finally, the state with the moving average can be modeled as follows:

$$\overline{\overline{\mathbf{z}}}_t = \sum_{k=1}^{K}\overline{\overline{\mathbf{g}}}_k\overline{\overline{b}}_k e^{\overline{\overline{\omega}}_k t}. \tag{26}$$

Herein, $\overline{\overline{\mathbf{z}}}_t$ refers to the smoothed version of the original signal at time t after applying the moving average filter to the received data. $\overline{\overline{\mathbf{g}}}_k$ means the dynamic modes of the system, obtained from the eigenvectors of the mapping matrix $\overline{\overline{\mathbf{F}}}$ in the low-rank projection space. $\overline{\overline{b}}_k$ is the amplitudes associated with the dynamic mode $\overline{\overline{\mathbf{g}}}_k$. $\overline{\overline{\omega}}_k$ corresponds to the frequencies associated with each dynamic mode, which is derived from the eigenvalues of $\overline{\overline{\mathbf{F}}}$. It is clear that the signal $\overline{\overline{\mathbf{z}}}_t$ represents the reconstructed signal that captures the underlying dynamics of the system while mitigating the Gaussian white noise interference. When signal properties are unknown, the moving average window size can be initialized from a coarse spectral estimate of the interference bandwidth and refined by minimizing the reconstruction error.

C. Moving Average-Hankel-Dynamic Mode Decomposition

After applying the moving average filter, we focus on the spatial modes and their Hankel matrix construction for the augmented DMD analysis. To facilitate the augmented DMD analysis, we construct the Hankel matrix using the moving-averaged states. This approach enables effective separation of distinct dynamic modes, which is particularly crucial for accurate DOA estimation. The Hankel matrix is formed by systematically stacking spatially shifted copies of the measurement sequence.

In particular, we first define the spatial mode $\overline{\overline{\mathbf{s}}}_k$ after applying the moving average filter to the system's original state. The k-th spatial mode $\overline{\overline{\mathbf{s}}}_k$ is defined as

$$\overline{\overline{\mathbf{s}}}_k = \overline{\overline{\mathbf{g}}}_k\overline{\overline{b}}_k = \left[\overline{\overline{s}}_1, \cdots, \overline{\overline{s}}_l, \cdots, \overline{\overline{s}}_L\right]^T \in \mathbb{C}^{L\times 1}, \tag{27}$$

where $\overline{\overline{\mathbf{g}}}_k$ is the dynamic mode for the k-th source. $\overline{\overline{b}}_k$ is the amplitude corresponding to the k-th mode. L is the total number of sensors in the ULA system.

Next, we shift the spatial modes into the corresponding Hankel matrix by stacking sliding windows of the spatial modes, which is obtained as follows:

$$\overline{\overline{\mathbf{S}}}_{\mathrm{H}} = \begin{bmatrix} \overline{\overline{s}}_1 & \overline{\overline{s}}_2 & \cdots & \overline{\overline{s}}_{L-c} & \overline{\overline{s}}_{L-c+1} \\ \overline{\overline{s}}_2 & \overline{\overline{s}}_3 & \cdots & \overline{\overline{s}}_{L-c+1} & \overline{\overline{s}}_{L-c+2} \\ \vdots & \vdots & \ddots & \vdots & \vdots \\ \overline{\overline{s}}_c & \overline{\overline{s}}_{c+1} & \cdots & \overline{\overline{s}}_{L-1} & \overline{\overline{s}}_L \end{bmatrix}. \tag{28}$$

Each row of this Hankel matrix, $\overline{\overline{\mathbf{S}}}_{\mathrm{H}}$, corresponds to an augmented snapshot of the spatial modes. c is the number of space delays used to shift the window of spatial modes. A typical choice is to set c lager than the number of the signal and tones. Thus it must satisfy $c \geq 2$ to properly characterize each spatial mode. We proceed with the decomposition of this Hankel matrix $\overline{\overline{\mathbf{S}}}_{\mathrm{H}}$ to extract the augmented system's dynamic modes and their corresponding spatial frequencies information. Similar to the DMD method, we first sort the $\overline{\overline{\mathbf{S}}}_{\mathrm{H}}$ into two adjacent matrices as follows:

$$\overline{\overline{\mathbf{S}}}_{\mathrm{H}}^1 = \begin{bmatrix} \overline{\overline{s}}_1 & \overline{\overline{s}}_2 & \cdots & \overline{\overline{s}}_{L-c} \\ \overline{\overline{s}}_2 & \overline{\overline{s}}_3 & \cdots & \overline{\overline{s}}_{L-c+1} \\ \vdots & \vdots & \ddots & \vdots \\ \overline{\overline{s}}_c & \overline{\overline{s}}_{c+1} & \cdots & \overline{\overline{s}}_{L-1} \end{bmatrix}, \tag{29}$$

$$\overline{\overline{\mathbf{S}}}_{\mathrm{H}}^2 = \begin{bmatrix} \overline{\overline{s}}_2 & \overline{\overline{s}}_3 & \cdots & \overline{\overline{s}}_{L-c+1} \\ \overline{\overline{s}}_3 & \overline{\overline{s}}_4 & \cdots & \overline{\overline{s}}_{L-c+2} \\ \vdots & \vdots & \ddots & \vdots \\ \overline{\overline{s}}_{c+1} & \overline{\overline{s}}_{c+2} & \cdots & \overline{\overline{s}}_L \end{bmatrix}. \tag{30}$$

Also, we assume that adjacent columns in the matrix $\overline{\overline{\mathbf{S}}}_{\mathrm{H}}$ are related by a mapping function. This relationship can be expressed in the following matrix form, $\overline{\overline{\mathbf{S}}}_{\mathrm{H}}^2 = \overline{\overline{\mathbf{F}}}_{\mathrm{H}}\overline{\overline{\mathbf{S}}}_{\mathrm{H}}^1$. We start by performing SVD on $\overline{\overline{\mathbf{S}}}_{\mathrm{H}}^1$ as follows:

$$\overline{\overline{\mathbf{S}}}_{\mathrm{H}}^1 = \overline{\overline{\mathbf{U}}}_{\mathrm{H}}\,\overline{\overline{\mathbf{\Sigma}}}_{\mathrm{H}}\,\overline{\overline{\mathbf{V}}}_{\mathrm{H}}^*, \tag{31}$$

where $\overline{\overline{\mathbf{U}}}_{\mathrm{H}}$ and $\overline{\overline{\mathbf{V}}}_{\mathrm{H}}$ are the left and right singular vectors, respectively. $\overline{\overline{\mathbf{\Sigma}}}_{\mathrm{H}}$ is the diagonal matrix of singular values. Next, the mapping matrix $\overline{\overline{\mathbf{F}}}_{\mathrm{H}}$ can be derived as

$$\overline{\overline{\mathbf{F}}}_{\mathrm{H}} = \overline{\overline{\mathbf{S}}}_{\mathrm{H}}^2\,\overline{\overline{\mathbf{V}}}_{\mathrm{H}}\,\overline{\overline{\mathbf{\Sigma}}}_{\mathrm{H}}^{-1}\overline{\overline{\mathbf{U}}}_{\mathrm{H}}^*. \tag{32}$$

Finally, the augmented state in the Hankel matrix $\overline{\overline{\mathbf{s}}}_c$ can be modeled as:

$$\overline{\overline{\mathbf{s}}}_c = \sum_{q=1}^{Q}\overline{\overline{\mathbf{g}}}_q^{\mathrm{H}}\overline{\overline{b}}_q^{\mathrm{H}} e^{\overline{\overline{\omega}}_q^{\mathrm{H}} l}, \tag{33}$$

where $\overline{\overline{\mathbf{g}}}_q^{\mathrm{H}}$ represents the eigenvector associated with the q-th dynamic mode, $\overline{\overline{\omega}}_q^{\mathrm{H}}$ is the eigenvalue corresponding to the frequency for the k-th mode, $\overline{\overline{b}}_q^{\mathrm{H}}$ is the amplitude associated with the q-th mode. The DOA is derived from the eigenvalue $\overline{\overline{\omega}}_q^{\mathrm{H}}$. This allows us to pair the DOA and frequency, facilitating the identification of the SOI and the separation from RFI. As a result, the angle information can be effectively extracted, allowing clear separation of the SOI from both RFI and additive Gaussian white noise. Fig. 2 shows the flowchart of the proposed MAHankDMD method. It is worth noting that

MAHankDMD assumes the RFI and source signal occupy distinct frequency bands. If their frequency components overlap significantly or coincide, the method may fail to separate them, as the distinction relies on spectral differences. In addition, MAHankDMD remains effective in separating the SOI from RFI even when both signals share the same DOA, as long as they exhibit different frequencies. Classical methods such as MUSIC and ESPRIT rely on assumptions of spatially white noise and uncorrelated sources, making them unsuitable for scenarios with the RFI, where they fail to distinguish structured interference from the SOI.

IV. Results

In this section, we comprehensively evaluate the proposed MAHankDMD method for joint DOA and frequency estimation in the presence of RFI and Gaussian white noise.

A. Moving Average Filter for Frequency Estimation in the Presence of Gaussian White Noise

To investigate the performance of the MAHankelDMD method for frequency estimation in the presence of Gaussian white noise, we simulate a scenario in which a ULA receives signals from multiple sources and RFIs, with added Gaussian white noise. The SOI configuration includes $N = 2$, $\theta_1^1 = 30°, \omega_1^1 = 2$ GHz, $\theta_2^1 = 45°, \omega_2^1 = 2$ GHz. The RFI sources are defined by $J = 2$, $\theta_1^2 = 20°, \omega_1^2 =$5 GHz, $\theta_2^2 = 60°, \omega_2^2 = 5$ GHz. Six different SNR levels were simulated, which includes -3 dB, -1 dB, 1 dB, 3 dB, 5 dB, and 7 dB. Each configuration is evaluated through 500 Monte Carlo trials. In this example, the total time sequence length was set to 300, and a moving average filter with ζ=20 was applied, effectively smoothing the data before performing the MAHankDMD analysis.

Fig. 3 presents the frequency estimation results obtained by the conventional DMD and the proposed MAHankDMD methods under the six SNR conditions. Note that the obtained eigenvalues are complex numbers, where the imaginary part corresponds to the frequencies and the real part to the damping factors. To further examine the robustness limits of MAHankDMD, we extended the simulations to more challenging noise conditions, i.e., SNR = -7 dB, -9 dB, and -11 dB, whose result is plotted in Fig. 4. It is clear that the method maintains reliable frequency estimation capability up to SNR = -9 dB. For a more intuitive comparison, the mean absolute error (MAE) of the estimated frequencies is plotted in Fig. 5. The results demonstrate that for both DMD and MAHankDMD, frequency estimation accuracy improves as the noise level decreases, which aligns with expectations. Importantly, across all SNR levels, the MAHankDMD method consistently achieves lower MAE values when compared to the conventional DMD, indicating superior performance. In particular, under low SNR conditions such as -3 dB and -1 dB, the DMD method exhibits significant estimation errors, often failing to produce accurate frequency estimates. In contrast, the MAHankDMD method remains robust, highlighting its effectiveness in handling strong Gaussian white noise environments. It is clear that the incorporation of the moving average step effectively suppresses random fluctuations caused by Gaussian white noise and significantly improves the overall estimation performance, particularly in low-SNR scenarios. Hence, we can conclude that the proposed MAHankDMD method demonstrates strong robustness and superior accuracy for frequency estimation under varying levels of Gaussian white noise, making it a reliable solution in noisy environments.

B. Effect of Varying Window Size in Moving Average

To further investigate the impact of the moving average filter on the performance of frequency estimation, we explore how different window sizes ζ influence the accuracy of the proposed MAHankDMD method. The same simulation scenario as described previously is adopted, with two SOI sources and two RFI sources impinging on a ULA of 9 antennas, under the presence of additive Gaussian white noise. The frequency and angular parameters remain unchanged, and the SNR is fixed at a moderate level of 3 dB to ensure sensitivity to changes in denoising performance. We evaluate different window sizes for the moving average filter: $\zeta = 1, 5, 10, 15, 20, 25, 30, 35, 40, 45, 50$. Note that $\zeta = 1$ corresponds to the case without any moving average filtering. For each simulation, 500 Monte Carlo trials are performed, and the MAE of the estimated frequencies is calculated to assess accuracy.

Fig. 6 illustrates the effect of varying the window size ζ in the moving average filter on the mean absolute error (MAE) of frequency estimation using the proposed MAHankDMD method. The x-axis denotes the number of points in the moving average window, while the y-axis represents the corresponding MAE of the estimated frequencies. The bar chart shows the MAE for each tested window size, with an overlaid orange line and diamond markers depicting the overall trend. As observed, the MAE is substantially high when no averaging is applied ($\zeta = 1$), indicating poor estimation accuracy in noisy environments. As the window size increases, the MAE decreases rapidly, reaching its lowest values in the range of $\zeta = 20$ to $\zeta = 30$. This indicates that moderate smoothing effectively reduces noise while preserving essential signal dynamics. However, beyond $\zeta = 35$, the MAE begins to rise again. This degradation is likely due to the excessive smoothing effect, which distorts the underlying temporal structure of the signal and hampers accurate frequency extraction. This U-shaped trend highlights the critical importance of selecting an appropriate window size to strike a balance between noise suppression and signal fidelity within the MAHankDMD framework. The results suggest that a window size of $\zeta = 20$ offers an optimal trade-off in our simulation setting, yielding the best overall performance. Therefore, careful tuning of the moving average window size is recommended when applying the MAHankDMD method in practical noisy environments to ensure reliable and accurate frequency estimation.

C. Two SOIs with Two RFI Sources

To verify the proposed method, we first consider an example of the interference model of two SOIs with two RFI sources, as shown in (8). Specifically for this first part of our model

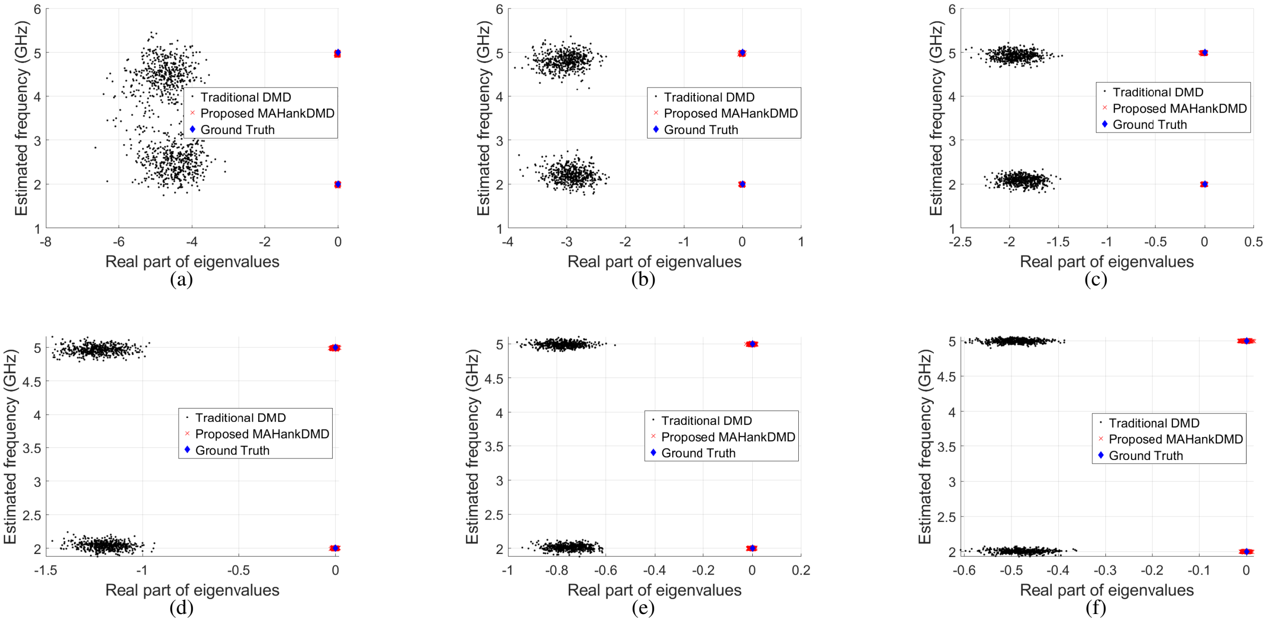

Fig. 3. Comparison of frequency estimation results between DMD and MAHankDMD methods in the presence of different Gaussian white noise environments: SNR = (a) -3 dB, (b) -1 dB, (c) 1 dB, (d) 3 dB, (e) 5 dB, and (f) 7 dB.

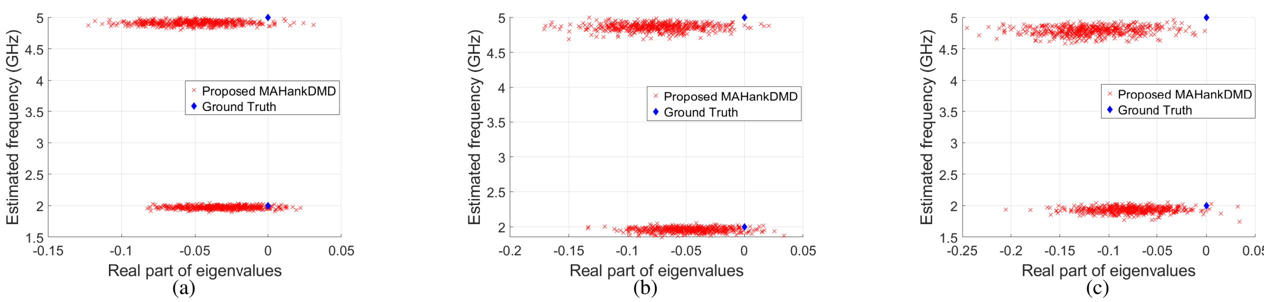

Fig. 4. Frequency estimation results obtained by MAHankDMD methods with SNR = (a) -7 dB, (b) -9 dB, (c)-11 dB.

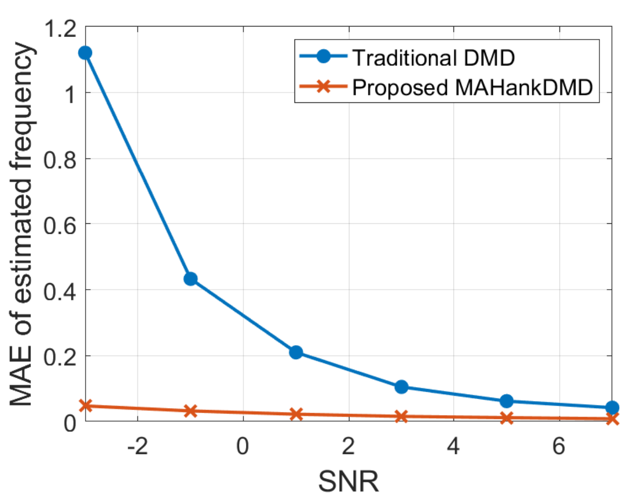

Fig. 5. Comparison of MAE of the estimated frequency between the traditional DMD and the proposed MAHankDMD method, where SOI configuration includes $N = 2$, $\theta_1^1 = 30°, \omega_1^1 = 2$ GHz, $\theta_2^1 = 45°, \omega_2^1 = 2$ GHz. The RFI sources are defined by $J = 2$, $\theta_1^2 = 20°, \omega_1^2 =$5 GHz, $\theta_2^2 = 60°, \omega_2^2 = 5$ GHz.

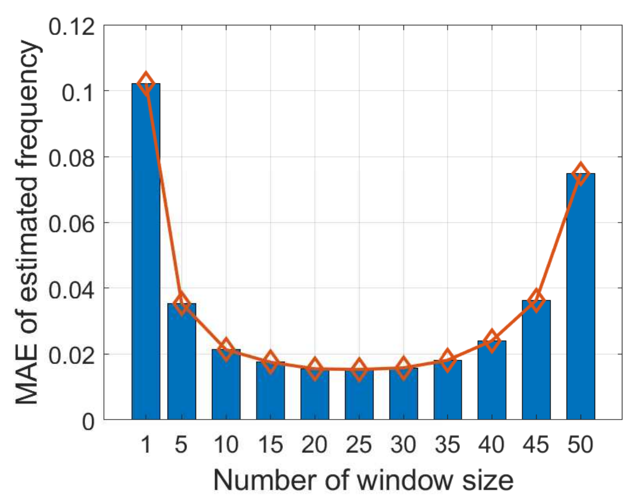

Fig. 6. Illustration of varying the window size ζ in the moving average filter on the MAE of frequency estimation using the MAHankDMD method, where the configuration is the same as Fig. 5.

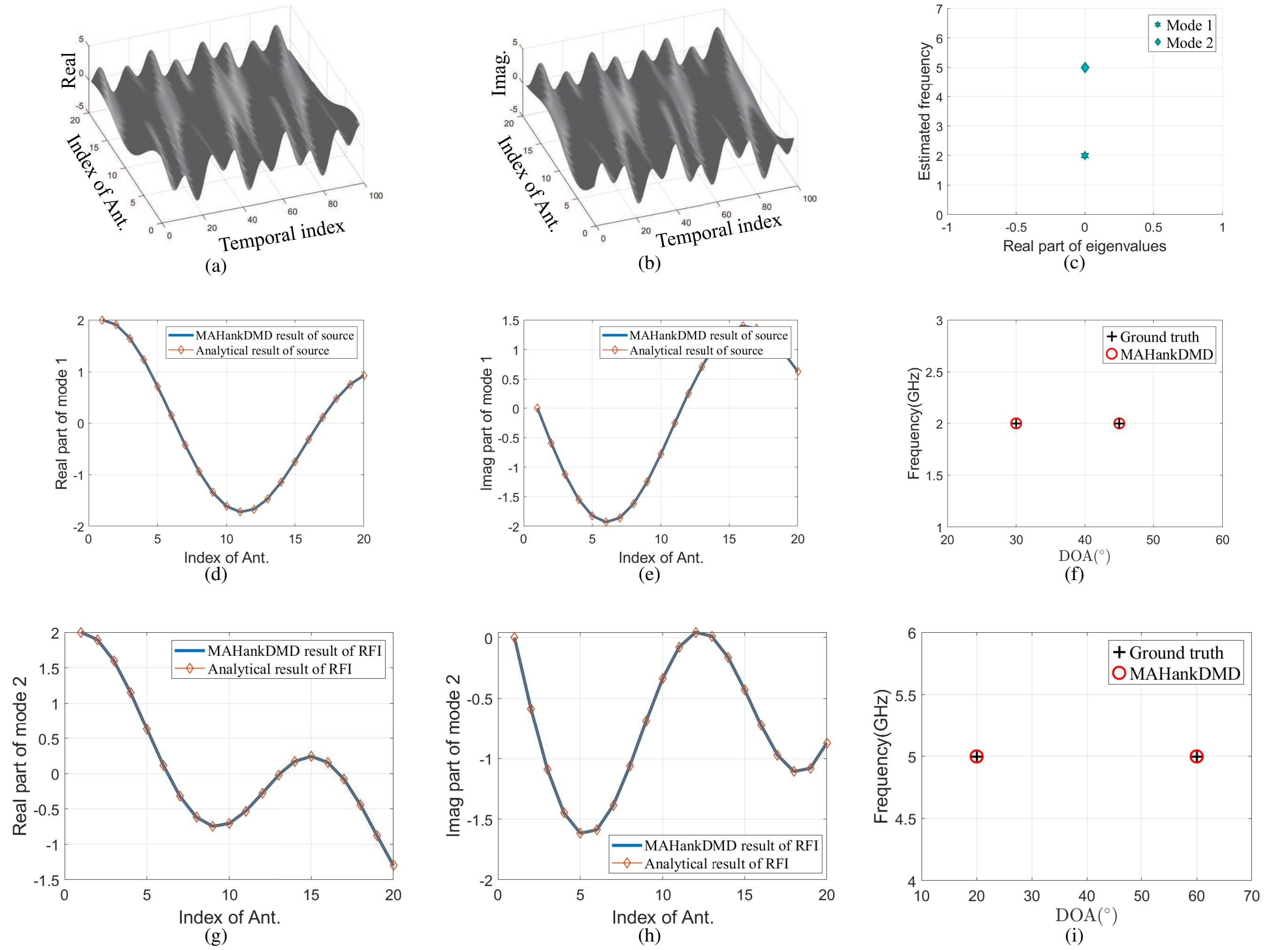

Fig. 7. Analysis results of interference model: (a) real part of the distribution of original data, (b) imaginary part of distribution of original data, (c) distribution of MAHankDMD eigenvalues, (d) comparison of the real distribution of extracted mode 1 and the analytical solution of source, (e) comparison of the imaginary distribution of extracted mode 1 and the analytical solution of source, (f) joint estimation result for the source: $N = 2$, $\theta_1^1 = 30°, \omega_1^1$ =2 GHz, $\theta_1^1 = 45°, \omega_2^1 = 2$ GHz, (j) comparison of the real distribution of extracted mode 2 and the analytical solution of the RFI, (h) comparison of the imaginary distribution of extracted mode 2 and the analytical solution of the RFI, (i) joint estimation result for the RFI: $J = 2$, $\theta_1^2 = 20°, \omega_1^2$ =5 GHz, $\theta_2^2 = 60°, \omega_2^2 = 5$ GHz.

regarding the SOIs, the parameters are set as $N = 2$, $\theta_1^1 = 30°, \omega_1^1 = 2$ GHz, $\theta_2^1 = 45°, \omega_2^1 = 2$ GHz, and for the RFI sources the configuration parameters are $J = 2$, $\theta_1^2 = 20°, \omega_1^2$ =5 GHz, $\theta_2^2 = 60°, \omega_2^2 = 5$ GHz. The ULA comprises 20 antennas. The sampling frequency is 10 GHz, and the sampling period is 10 ns. Therefore, 100 points are sampled in the time dimension. Then, the received spatial-temporal signal has a dimension of 20×100.

The MAHankDMD method decomposes the received signal into eigenvector components and their corresponding spatial modes. Fig. 7(a) and (b) display the real and imaginary parts of the original spatial-temporal data, while Fig. 7(c) presents the distribution of the eigenvalues derived from the MAHankDMD method. Clearly, the estimated frequencies corresponding to each mode are correctly identified at 2 GHz and 5 GHz. To evaluate the accuracy of spatial mode estimation, Fig. 7(d) and (e) compare the real and imaginary parts of the extracted dynamic mode associated with the SOIs (mode 1) against the analytical solution. A high degree of agreement is observed. Similarly, Fig. 7(g) and (h) show the comparison for the second mode corresponding to the RFI components, again demonstrating excellent consistency. The results of the joint frequency and DOA estimation are shown in Fig. 7(f) and (i) for the SOIs and RFIs, respectively. The estimated values using MAHankDMD closely match the ground truth, confirming the accuracy and effectiveness of the proposed method in extracting both frequency and spatial information in the presence of strong interference. In summary, the results clearly demonstrate that the proposed MAHankDMD method can accurately estimate the frequency and DOA of multiple signal components in the presence of strong radio frequency interference and Gaussian white noise. The extracted dynamic modes align closely with analytical solutions in both the real and imaginary domains, and the joint estimation results for frequency and DOA show excellent agreement with ground truth values. These findings validate the robustness and relia-

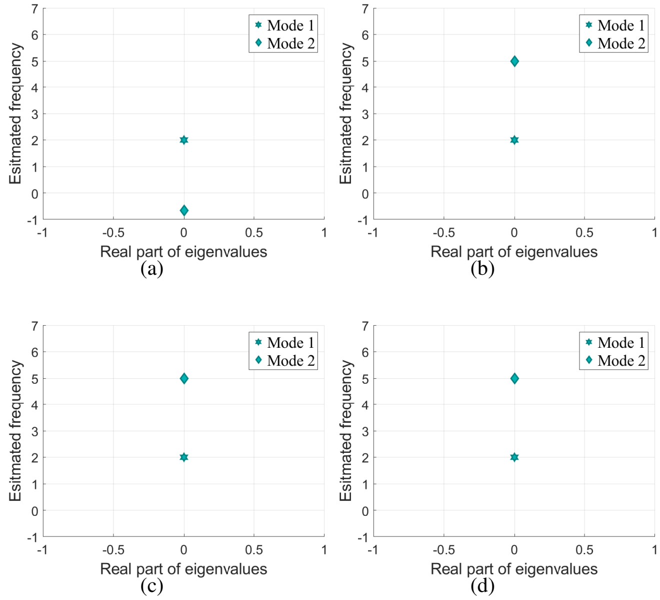

Fig. 8. Frequency estimation performance of the MAHankDMD method at different sampling frequencies: (a) 1 GHz, (b) 2 GHz, (c) 5 GHz, and (d) 10 GHz.

bility of MAHankDMD in separating and identifying sources and interfering signals in complex noisy environments.

D. Estimation with Subsampling

For further verification, we investigate the effect of subsampling using the same parameter settings as in Fig. 7. Fig. 8(a)-(d) respectively illustrate the distribution of MAHankDMD eigenvalues at sampling frequencies of 1 GHz, 2 GHz, 5 GHz, and 10 GHz. As shown in Fig. 8(a), the estimation results at 1 GHz are inaccurate, indicating that a 1 GHz sampling rate is insufficient for accurate spectral analysis. In contrast, Figs. 8(b)-(d) reveal that at 2 GHz, 5 GHz, and 10 GHz, the eigenvalue distributions exhibit well-defined mode structures, allowing correct frequency characteristics to be recovered. Notably, the Nyquist rate for the original signal is 10 GHz; however, unlike traditional Fourier-based methods [34], which rely on orthogonal basis projections and require Nyquist-compliant sampling, the proposed MAHankDMD method does not impose this constraint. It remains effective even when applied to subsampled data. These results demonstrate that the MAHankDMD method can accurately estimate both DOA and frequency in the presence of noise and interference, even under subsampling conditions. This capability reduces the demand for high-rate data acquisition, thereby mitigating dependence on expensive or high-performance hardware components.

E. Performance

To further validate the effectiveness and robustness of the proposed MAHankDMD method under noisy environments, a comprehensive noise analysis was conducted. Fig. 9(a) and (b) illustrate the root mean square error (RMSE) of frequency estimation as a function of signal-to-noise ratio (SNR), for the first frequency component $\omega_1^1 = 2$ GHz and the second frequency component $\omega_1^2 = 5$ GHz, respectively. Each subplot compares performance across four configurations of the ULA with different numbers of antenna elements: 12, 15, 18, and 20. As expected, the RMSE consistently decreases as the SNR increases, confirming that both frequencies are estimated more accurately under higher SNR conditions. This trend aligns well with theoretical expectations, as lower noise environments enable more reliable signal decomposition and dynamic mode extraction.

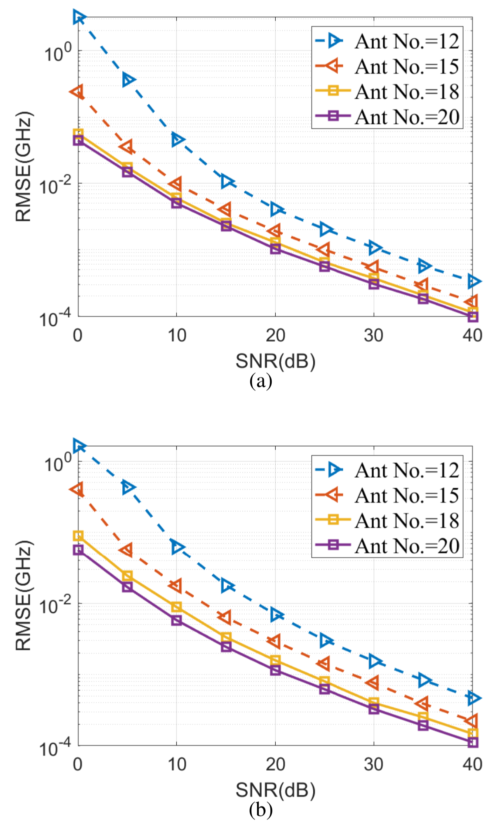

Fig. 9. RMSE versus SNR for (a) the first frequency, $\omega_1^1 = 2$ GHz, and (b) the second frequency, $\omega_1^2 = 5$, with different numbers of antennas.

In addition to the effect of noise, the number of antennas also plays a critical role in estimation accuracy. For any fixed SNR level, increasing the number of antennas leads to a significant reduction in RMSE for both frequency components. For instance, in low SNR regimes (e.g., 0-10 dB), the performance gap between 12 and 20 antennas is substantial, underscoring the importance of spatial diversity in overcoming noise and interference. Even in higher SNR conditions (e.g., above 30 dB), the improvement remains evident, albeit with a diminishing margin. This behavior can be attributed to the increased spatial resolution and array aperture provided by a larger antenna array, which enhances the ability of the MAHankDMD framework to extract accurate dynamic modes from the received data. A larger ULA enables finer discrimination of angular and spectral features, thereby improving both the frequency and DOA estimation. Hence, these results confirm the dual importance of both high SNR and sufficient antenna elements in achieving reliable performance with the MAHankDMD method. The method not only remains robust across varying noise levels but also benefits significantly from increased spatial sampling, making it highly suitable for practical array signal processing applications under diverse operational conditions.

V. Conclusions

In this work, we introduced the MAHankDMD method for joint DOA and frequency estimation in environments affected by both RFI and white noise. By combining the moving average filter for noise suppression with the Hankel-DMD approach for DOA estimation, the proposed method effectively mitigates the impact of Gaussian white noise, allowing for accurate separation of the SOI from interference. Numerical simulations validate the robustness of MAHankDMD, demonstrating its capability to reliably estimate DOA and frequency even in complex noisy environments. MAHankDMD provides a powerful, data-driven solution that enhances signal estimation accuracy and offers a promising tool for cognitive radio and wireless communication systems that face interference even more nowadays. Our method is well-suited for integrated sensing and communication systems, where reliable joint DOA and frequency estimation is required under noisy and interfered conditions.

References

[1] A. M. Molaei, P. del Hougne, V. Fusco, and O. Yurduseven, "Efficient joint estimation of DOA, range and reflectivity in near-field by using mixed-order statistics and a symmetric MIMO array," *IEEE Trans. Veh. Technol.*, vol. 71, no. 3, pp. 2824–2842, 2022.

[2] S. Uehashi, Y. Ogawa, T. Nishimura, and T. Ohgane, "Prediction of time-varying multi-user MIMO channels based on DOA estimation using compressed sensing," *IEEE Trans. Veh. Technol.*, vol. 68, no. 1, pp. 565–577, 2019.

[3] W. Li and J. Qi, "Multitarget three-dimensional location estimation based on phaseless measurements by double metasurface antennas," *IEEE Internet Things J.*, 2024.

[4] Y. Hou and W.-Q. Wang, "Active frequency diverse array counteracting interferometry-based DOA reconnaissance," *IEEE Antennas Wirel. Propag. Lett.*, vol. 18, no. 9, pp. 1922–1925, 2019.

[5] L. Liu and P. Wei, "Joint DOA and frequency estimation with sub-nyquist sampling in the sparse array system," *IEEE Signal Process. Lett.*, vol. 25, no. 9, pp. 1285–1289, 2018.

[6] G. Verma, F. T. Dagefu, B. M. Sadler, and J. Twigg, "Direction of arrival estimation with the received signal strength gradient," *IEEE Trans. Veh. Technol.*, vol. 67, no. 11, pp. 10856–10870, 2018.

[7] S. Jiang, N. Fu, Z. Wei, X. Li, L. Qiao, and X. Peng, "Joint spectrum, carrier, and DOA estimation with beamforming MWC sampling system," *IEEE Trans Instrum. Meas.*, vol. 71, pp. 1–15, 2022.

[8] M. F. Imani and I. Alamzadeh, "Conformal frequency-diverse metasurface for computational AoA detection," *IEEE Antennas Wirel. Propag. Lett.*, 2023.

[9] J.-D. Lin, W.-H. Fang, Y.-Y. Wang, and J.-T. Chen, "FSF MUSIC for joint DOA and frequency estimation and its performance analysis," *IEEE Trans. Signal Process.*, vol. 54, no. 12, pp. 4529–4542, 2006.

[10] J. Shi, D.-S. Yang, S.-G. Shi, Z. rui Zhu, and B. Hu, "Spatial time-frequency DOA estimation based on joint diagonalization using Jacobi rotation," *Appl. Acoust*, vol. 116, pp. 24–32, 2017.

[11] M. Viberg and P. Stoica, "A computationally efficient method for joint direction finding and frequency estimation in colored noise," in *Conference Record of Thirty-Second Asilomar Conference on Signals, Systems and Computers (Cat. No.98CH36284)*, vol. 2, pp. 1547–1551 vol.2, 1998.

[12] S. S. Ioushua, O. Yair, D. Cohen, and Y. C. Eldar, "CaSCADE: Compressed carrier and DOA estimation," *IEEE Trans. Signal Process.*, vol. 65, no. 10, pp. 2645–2658, 2017.

[13] S. Wang, J. Caffery, and X. Zhou, "Analysis of a joint space-time DOA/FOA estimator using MUSIC," in *12th IEEE International Symposium on Personal, Indoor and Mobile Radio Communications. PIMRC 2001. Proceedings (Cat. No. 01TH8598)*, vol. 1, pp. B–B, IEEE, 2001.

[14] A. Barthelme and W. Utschick, "A machine learning approach to DoA estimation and model order selection for antenna arrays with subarray sampling," *IEEE Trans. Signal Process.*, vol. 69, pp. 3075–3087, 2021.

[15] R. Varzandeh, K. Adiloğlu, S. Doclo, and V. Hohmann, "Exploiting periodicity features for joint detection and DOA estimation of speech sources using convolutional neural networks," in *ICASSP 2020-2020 IEEE International Conference on Acoustics, Speech and Signal Processing (ICASSP)*, pp. 566–570, IEEE, 2020.

[16] A. Aich and P. Palanisamy, "On-grid DOA estimation method using orthogonal matching pursuit," in *2017 International Conference on Signal Processing and Communication (ICSPC)*, pp. 483–487, IEEE, 2017.

[17] Y. Zhang and L. Jiang, "A direct data approach to joint 2-D DOA and frequency estimation with l-shaped array," *IEEE Trans. Aerosp. Electron. Syst.*, vol. 59, no. 4, pp. 3684–3694, 2023.

[18] Z. Dai, J. Yin, W. Men, L. Zhang, and Z. Jiang, "A variable threshold parameter Andrews sine estimator for DOA estimation under impulsive noise," *IEEE Trans. Instrum. Meas.*, 2025.

[19] A. M. Maras, "Locally optimum detection in moving average non-Gaussian noise," *IEEE Trans. Commun.*, vol. 36, no. 8, pp. 907–912, 1988.

[20] J.-F. Gu, S. Chan, W.-P. Zhu, and M. Swamy, "Joint DOA estimation and source signal tracking with Kalman filtering and regularized QRD RLS algorithm," *IEEE Trans. Circuits Syst. II: Express Br.*, vol. 60, no. 1, pp. 46–50, 2013.

[21] S. Ouelha, A. Aissa-El-Bey, and B. Boashash, "Improving DOA estimation algorithms using high-resolution quadratic time-frequency distributions," *IEEE Trans. Signal. Process.*, vol. 65, no. 19, pp. 5179–5190, 2017.

[22] S. Salari, F. Chan, Y.-T. Chan, and R. Guay, "DOA estimation using compressive sampling-based sensors in the presence of interference," *IEEE Trans. Aerosp. Electron. Syst.*, vol. 56, no. 6, pp. 4395–4405, 2020.

[23] D. Zhu, J. Li, and G. Li, "RFI source localization in microwave interferometric radiometry: A sparse signal reconstruction perspective," *IEEE Trans. Geosci. Remote Sens.*, vol. 58, no. 6, pp. 4006–4017, 2020.

[24] X. Wei, D. Saha, G. Hellbourg, and A. Dutta, "Multistage 2D DoA estimation in low SNR," in *ICC 2023-IEEE International Conference on Communications*, pp. 2785–2790, IEEE, 2023.

[25] H. Jiang, J.-K. Zhang, and K. M. Wong, "Joint DOD and DOA estimation for bistatic MIMO radar in unknown correlated noise," *IEEE Trans. Veh. Technol.*, vol. 64, no. 11, pp. 5113–5125, 2015.

[26] A. Argyriou, "Multi-source cooperative communication with opportunistic interference cancelling relays," *IEEE Trans. Commun.*, vol. 63, no. 11, pp. 4086–4096, 2015.

[27] S. Guan, J. Li, and X. Luo, "Variational bayesian gaussian mixture model for off-grid DOA estimation," *Electron. Lett.*, vol. 60, no. 3, p. e13114, 2024.

[28] O. M. Abdelrhman, S. Li, Y. Dou, and L. Bin, "Robust total maximum versoria algorithm for efficient DOA estimation in noisy inputs," *IEEE Trans. Veh. Technol.*, 2024.

[29] C. Wang, X. Cui, G. Liu, and M. Lu, "Two-stage spatial whitening and normalized MUSIC for robust DOA estimation of GNSS signals under jamming," *IEEE Trans. Aerosp. Electron. Syst.*, 2024.

[30] Y. Zhang, W. Xu, A.-L. Jin, M. Li, P. Ma, L. Jiang, and S. Gao, "Coupling-informed data-driven scheme for joint angle and frequency estimation in uniform linear array with mutual coupling present," *IEEE Trans. Antennas Propag.*, vol. 72, no. 12, pp. 9117–9128, 2024.

[31] Y. Zhang and L. Jiang, "A novel data-driven method for two-dimensional angles finding via uniform rectangular array with automatic pairing," *IEEE Trans. Veh. Technol.*, vol. 72, no. 2, pp. 1972–1981, 2023.

[32] Y. Zhang, L. Jiang, and H.-T. Chou, "Data-driven scheme for joint estimation of direction-of-arrival and frequency with uniform linear array," *IEEE Trans. Veh. Technol.*, vol. 72, pp. 15706–15718, Dec. 2023.

[33] Z. Shan, J. Yang, M. A. Sanjuán, C. Wu, and H. Liu, "A novel adaptive moving average method for signal denoising in strong noise background," *Europ. Phys. J. Plus*, vol. 137, no. 1, p. 50, 2022.

[34] S.-T. Yang and H. Ling, "Design of a microstrip leaky-wave antenna for two-dimensional bearing tracking," *IEEE Antennas Wirel. Propag. Lett.*, vol. 10, pp. 784–787, 2011.